

# ACTIVE CONTROLS IN INTERFEROMETRIC DETECTORS OF GRAVITATIONAL WAVES: INERTIAL DAMPING OF THE VIRGO SUPERATTENUATOR\*

GIOVANNI LOSURDO

*Istituto Nazionale di Fisica Nucleare - Sezione di Pisa*  
E-mail: losurdo@galileo.pi.infn.it

The operation of an interferometer for gravitational waves detection requires sophisticated feedback controls in many parts of the apparatus. The aim of this lecture is to introduce the types of problems to be faced in this line of research. The attention is focused on the *inertial damping* of the test mass suspension of the VIRGO interferometer (the superattenuator): it is a multidimensional local control aimed to reduce the residual motion of the suspended mirror associated to the normal modes of the suspension. Its performance is very important for the locking of the interferometer.

## 1 Introduction

Operating an interferometer for gravitational waves detection requires the implementation of many active controls on the different parts of the apparatus. For instance, feedback controls are needed to reduce the laser frequency and power fluctuations, to keep the optical cavities in resonance and to maintain the interferometer output on a dark fringe. The basic idea is that the apparatus works at its best strictly around a well defined working point <sup>1</sup> (laser fluctuations and shot noise at a minimum, optical cavities in resonance and interferometer output on a dark fringe). Internal and external disturbances overload the dynamic range of the interferometer. Therefore, the system has to be forced to remain in the correct working position. This is achieved via feedback controls.

In this lecture we examine in detail one of the controls needed to reach the final goal of operating the interferometer: the *inertial damping* of the VIRGO superattenuator (SA) <sup>3</sup>. The SA can be described as a chain of mechanical “filters”, each one acting as a “spring” in 6 degrees of freedom. The normal mode frequencies of the SA range between 0.04 and about 2 Hz. At frequencies  $f >> 2$  Hz the SA acts as a steep filter of the seismic vibrations of the ground (an attenuation factor of  $10^{15}$  @ 10 Hz is expected). Therefore,

---

\*LECTURE GIVEN AT THE INTERNATIONAL SUMMER SCHOOL ON EXPERIMENTAL PHYSICS OF GRAVITATIONAL WAVES - URBINO (ITALY), SEPTEMBER 6-18, 1999

in the interferometer detection band (10 Hz-few kHz), the suspended mirror is “disconnected” from the ground. Beside being a low pass filter for ground vibrations the SA is a tool for actively controlling the mirror position. Forces that move and steer the mirror can be exerted in 3 points of the SA chain: the inverted pendulum (IP)<sup>5</sup>, the *marionetta* (a special mechanical tool designed to steer the mirror) and the mirror itself (from a suspended *reference mass*).

Keeping the interferometer in the operating position requires the mirror to have a maximum RMS relative motion of less the  $10^{-12}$  m. In the frequency range where the SA is fully effective ( $f >> 4$  Hz) the residual motion of the mirror is negligible. On the other hand, the mirror free motion in the region of the SA normal modes is  $\sim 100$   $\mu$ m. Feedback forces acting on the SA must reduce the mirror motion from  $100$   $\mu$ m to  $10^{-12}$  m. The dynamic range of a feedback system able to perform this control has to be huge: the control is performed in three steps (hierarchical control<sup>2</sup>). The first step is a damping of the SA normal modes in order to reduce the mirror residual motion to less than  $10$   $\mu$ m. This is necessary in order to control the mirror position acting on the lower stages without reinjecting noise into the detection band. We describe in the following an implementation of a high gain and wideband damping of the SA resonances.

## 2 Experimental setup

The setup (fig. 1) of the experiment is composed of a full scale superattenuator, provided with 3 accelerometers (placed on the top of the IP), 3 LVDT position sensors (measuring the relative motion of the IP with respect to an external frame), 3 coil-magnet actuators. The accelerometers work in the range DC-400 Hz and have acceleration spectral sensitivity  $\sim 10^{-9}$  m s<sup>-2</sup> Hz<sup>-1/2</sup> below 3 Hz<sup>6</sup>. The sensors and actuators are all placed in *pin-wheel* configuration. The sensor and actuator signals are computer controlled by a ADC (16 bit)-DSP-DAC (20 bit) system. The DSP handles the signals of all the sensors and actuators. It can combine them by means of matrices, create complex feedback filters (like the one of fig. 8) with high precision poles/zeroes placement and perform all the calculations at a high sampling rate (10 kHz). The suspended mirror is also provided with LVDT position sensors to measure its displacement with respect to ground.

## 3 The approach to the problem of control

The IP, where all the sensors are placed and on which the forces are exerted, has 3 main resonant modes: two translation ( $X, Y$ ) and the rotation around

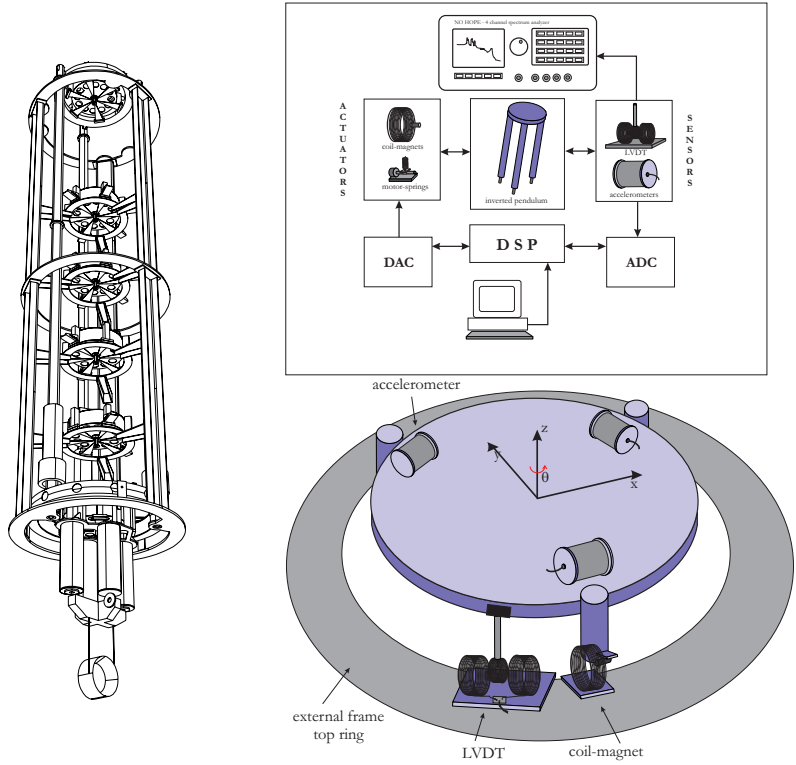


Figure 1. LEFT: the superattenuator; RIGHT TOP: logical scheme of the setup for the local active control; RIGHT BOTTOM: simplified view of the IP top table, provided with the 3 accelerometers. One LVDT position sensors and one coil-magnet actuator are also shown.

the vertical axis ( $\Theta$ ). Each sensor is sensitive to all the modes and each actuator can excite all the modes. In control theory language, such a system is defined MIMO (multiple in-multiple out). Controlling a MIMO system can be very difficult. Our approach has been different: the signals of the 3 sensors are digitally mixed (using proper transformation matrices) to build up *virtual sensors*, sensitive to one mode only and “blind” to the others. At the same time, we build up *virtual actuators* able to excite each mode separately. The system is thus uncoupled into 3 SISO (single in-single out) subsystems. In terms of analytical mechanics this means the system is described in the normal

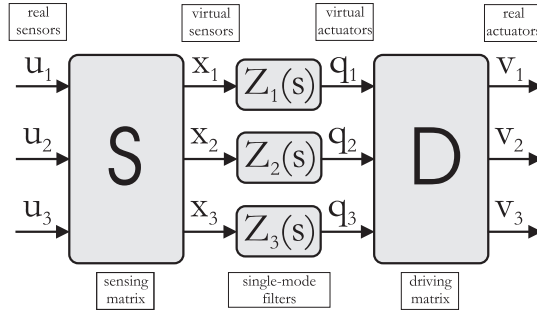


Figure 2. The logic of the diagonalisation: the output  $u_i$  of the sensors are linearly combined by a matrix  $\mathbf{S}$  in order to produce 3 *virtual* sensors outputs ( $x_i$ ), sensitive to pure modes. Three independent feedback filters  $Z_i(s)$  are designed for the pure modes and 3 generalized forces  $q_i$  are produced. The  $q_i$  are turned into real currents ( $v_i$ ) to feed the actuators via the matrix  $\mathbf{D}$ .

modes basis. The equations of motions take the form:

$$\ddot{x}_k + \omega_k^2 x_k = q_k \quad , \quad k = 1 \dots 3 \quad (1)$$

where  $x_k$  is the  $k$ -th normal mode,  $\omega_k/2\pi$  is the corresponding resonant frequency and  $q_k$  the generalized force on that mode. Let  $\mathbf{u} = (u_1, \dots, u_3)$  the vector made by the outputs of the 3 sensors and let  $\mathbf{x} = (x_1, \dots, x_3)$  the vector made by the 3 virtual sensors. Analogously, let  $\mathbf{v}$  the vector made by the 3 currents driving the actuators and  $\mathbf{q}$  the vector of the 3 generalized forces. The transformation from the system of the physical sensors/actuators to that of the virtual ones is operated by two matrices, such that:

$$\mathbf{v} = \mathbf{D}\mathbf{q} \quad (2)$$

$$\mathbf{x} = \mathbf{S}\mathbf{u} \quad (3)$$

The *sensing* ( $\mathbf{S}$ ) and *driving* ( $\mathbf{D}$ ) matrices are experimentally measured. The measurement procedure is described in details in ref. 9. The result of the measurement is determined by the mechanical characteristics of the system (resonant frequencies, quality factors), the geometry of the sensors and actuators and their calibration, but it is not needed to know them in order to measure the matrices. The logic of diagonalisation is explained by fig. 2.

After the diagonalisation the system can be considered as composed of 3 *uncoupled* oscillators, and the control strategy for each of them has to be defined independently (see fig. 3).

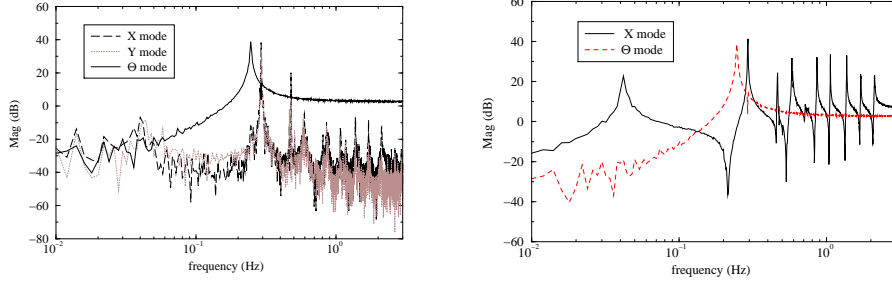


Figure 3. Effect of the digital diagonalisation. LEFT: the output of the 3 virtual accelerometers when  $\Theta$  is excited. RIGHT: the output of the virtual accelerometers  $X$  and  $\Theta$  are compared. Different feedback strategies are required in the two cases, because  $X$  senses all the translational modes of the SA chain.

#### 4 Inertial damping: principle

The control we describe here is called *inertial damping* because it is performed by using (mostly) *inertial sensors* (accelerometers). In the following, with the help of a simple model, we explain why this is the best choice to achieve a high performance damping.

Let us consider a simple pendulum of mass  $m$  and length  $l$ . Let  $x$  be the abscissa of the suspended mass,  $x_0$  that of the suspension point. Let  $F_{\text{fb}}$  the external force on the pendulum (i.e. the feedback force to control it). The equation of motion is then:

$$F_{\text{fb}} = m\ddot{x} + \gamma\dot{x} + k(x - x_0) \quad (4)$$

where  $\gamma$  is the viscous dissipation factor and  $k = mg/l$ . The control loop of such a system is sketched in fig. 4, where  $H(s)$  is the mechanical transfer function,  $G(s)$  is the compensator and  $out$  is the output of the sensor used. The goal of the control is to damp the pendulum resonance. This can be done easily with a *viscous* (theoretical) feedback force:

$$F_{\text{fb}} = -\gamma'\dot{x} \quad (5)$$

Our sensors do not measure  $x$ . Their output is:

$$out = \begin{cases} x - x_0 & \text{for displacement sensors} \\ \ddot{x} & \text{for accelerometers} \end{cases} \quad (6)$$

Therefore, the actual “viscous” force that can be built if position sensors are

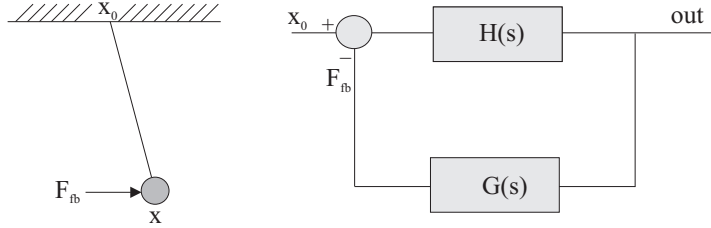


Figure 4. The control scheme for a simple pendulum

used has the form:

$$F_{fb}^p = -\gamma' \frac{d}{dt}(x - x_0) \quad (7)$$

It can be easily shown that with such a feedback force the closed loop equation of motion (in Laplace space) reduces to:

$$x(s) = \frac{\omega_0^2 + G_0 s}{s^2 + \omega_0^2 + (\omega_0/Q + G_0)s} \cdot x_0(s) \quad (8)$$

where  $G_0 = \gamma'/m$  is a gain parameter<sup>a</sup> measuring the intensity of the viscous feedback force, and  $Q$  is the open loop quality factor. When the loop is closed a damping of the resonance is achieved:

$$Q' \xrightarrow{G \gg 1} \frac{\omega_0}{G} \quad (9)$$

Nevertheless, as the gain is increased, a larger amount of noise is reinjected off-resonance. This is associated to the term “ $G_0 s$ ” in the numerator of (8) and depends on the fact that the sensor used to build up the feedback force measures the position of the pendulum with respect to ground. Therefore, an infinitely efficient feedback would “freeze” the pendulum to ground (which is seismic noisy), reducing its motion at the resonance, with the drawback of bypassing its attenuation properties above resonance.

The situation is fairly different when an inertial sensor is used. In this case the viscous feedback force is obtained by integrating the accelerometer output, and the output does not depend on  $x_0$ :

$$F_{fb}^a = -\gamma' \int \ddot{x} dt \quad (10)$$

<sup>a</sup>In a real feedback system a frequency dependent gain function  $G(s)$  rather than a gain parameter has to be considered.

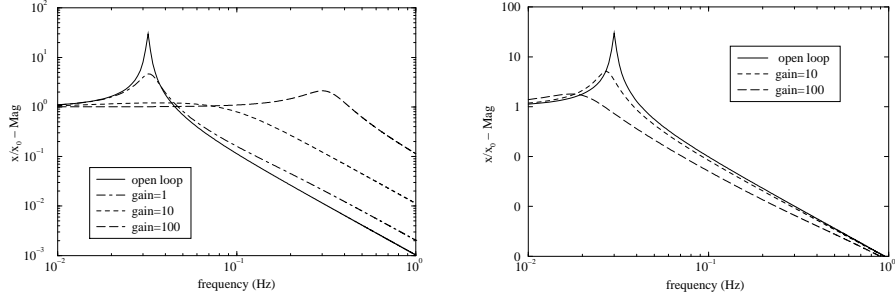


Figure 5. Damping of a simple pendulum: the closed loop transfer function  $x(s)/x_0(s)$  (magnitude) when a position sensor is used (LEFT) and when an accelerometer is used (RIGHT).

The closed loop equation of motion is then:

$$x(s) = \frac{\omega_0^2}{s^2 + \omega_0^2 + (\omega_0/Q + G_0)s} \cdot x_0(s) \quad (11)$$

A damping of the resonance is obtained (exactly as in the previous case) but without reinjection of off-resonance noise. In fig. 5 a simulation of the closed loop transfer function  $x(s)/x_0(s)$  is shown in the two cases. Up to now we have considered a simple viscous damping. It is possible to increase the bandwidth of the control if the feedback force contains a term proportional to  $x$  (the double integral of the accelerometer signal). The result obtained in this case is shown in fig. 6.

## 5 Control strategy

In this section we extend the principles of the previous section and describe the strategy to control the SA.

The basic idea of inertial damping is to use the accelerometer signal to build up the feedback force. As a matter of fact, an infinitely efficient feedback using only the inertial sensor information, would null the acceleration of the pendulum, but it would not do anything if the pendulum moves at constant velocity. Such a control would be unstable with respect to *drifts*. Therefore, if the control band is to be extended down to DC, a position signal is necessary. Our solution was a *merging* of the two sensors: the virtual LVDT (position) and accelerometer signals are combined in such a way that the LVDT signal ( $l(s)$ ) dominates below a chosen cross frequency  $f_{\text{merge}}$  while the accelerometer

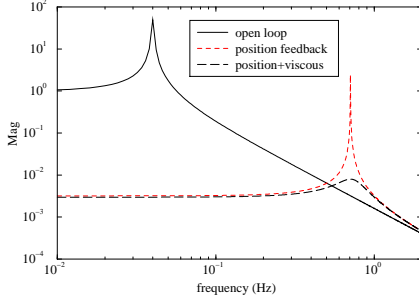


Figure 6. Inertial damping of a simple pendulum when a position feedback is implemented.

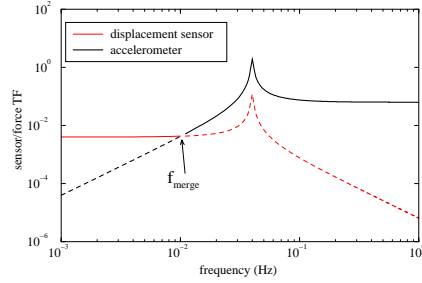


Figure 7. *Merging of displacement and acceleration sensors (simulation for a simple pendulum).*

signal ( $a(s)$ ) dominates above it (see fig. 7 and ref. 7). The feedback force has the form<sup>b</sup>:

$$F_{fb} = G(s) [a(s) + \epsilon l(s)] \quad (12)$$

where  $G(s)$  is the digital filter transfer function (see fig. 8) and  $\epsilon$  is the parameter whose value determines  $f_{\text{merge}}$ . We have chosen  $f_{\text{merge}} \sim 10$  mHz (corresponding to  $\epsilon \sim 5 \cdot 10^{-3}$ ). This approach stabilizes the system with respect to low frequency drifts at the cost of reinjecting a fraction  $\epsilon$  of the seismic noise via the feedback.

We describe in the following the feedback design for the 3 d.o.f., starting from the the translational ones. The virtual  $X$  and  $Y$  sensors show many resonant peaks (the modes of a chain of pendulums) and this requires a more sophisticated feedback strategy. The digital filter used to control the translation modes ( $G(s)$ ) is shown in fig. 8 (LEFT). It shows three main features:

- for  $0.01 < f < 2$  Hz the gain is proportional to  $f^{-2}$ . This corresponds to the case of fig. 6: the accelerometer signal is integrated twice and the feedback force is proportional to  $x$ ;
- for  $f > 2$  Hz the gain is proportional to  $f^{-1}$ . The accelerometer signal is integrated once: the feedback force is proportional to the velocity and a viscous damping is achieved;

<sup>b</sup>Actually, the LVDT signal  $l(s)$  is properly filtered in order to preserve feedback stability at the crossover frequency and in order to reduce the amount of reinjected noise at  $f > f_{\text{merge}}$ .

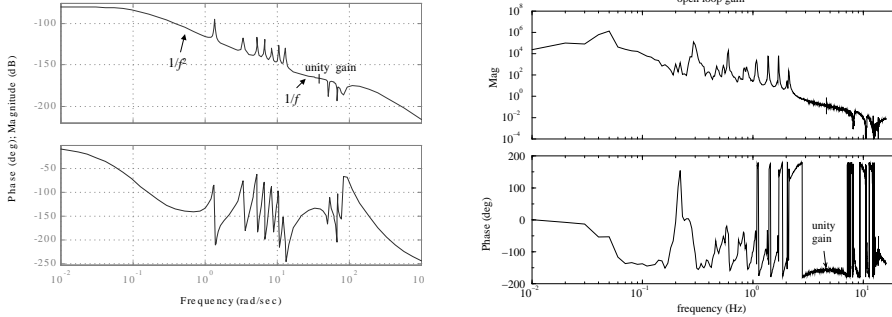


Figure 8. LEFT: Digital filter used for the inertial damping of a translation mode ( $X$ ). The filter slope is  $f^{-2}$  in the range  $10 \text{ mHz} < f < 3 \text{ Hz}$ ,  $f^{-1}$  for  $f > 3 \text{ Hz}$ . The unity gain is at 4 Hz. The peaks in the digital filter are necessary to compensate the dips in the mechanical transfer function (see the transfer function of the  $X$  mode in fig. 3). RIGHT: open loop gain function (measured). The phase margin at the unity gain frequency is about  $25^\circ$ .

- the peaks visible in the filter are necessary to compensate the corresponding dips in the mechanical transfer function ( $H(s)$ ) of fig. 3, in order to make the feedback stable.

Fig. 8 (RIGHT) shows the open loop gain transfer function  $G(s)H(s)$ .

The damping strategy for the  $\Theta$  mode is simpler: the  $\Theta$  virtual sensor (fig. 3, RIGHT) shows one resonance peak only and no dips: no compensation is necessary. Apart from this, the feedback strategy is similar to the ones used for the translational modes.

## 6 Inertial damping: experimental results

The result of the inertial control (on 3 d.o.f.) is shown in figure 9. The measurement has been performed in air. The noise on the top of the IP is reduced over a wide band (10 mHz - 4 Hz). A gain  $> 1000$  is obtained at the main SA resonance (0.3 Hz). The RMS translational motion of the IP (calculated as  $x_{\text{RMS}}(f) = \sqrt{\int_f^\infty \tilde{x}^2(\nu) d\nu}$ ) in 10 sec. is reduced from more than 30 to  $0.3 \mu\text{m}$ . The closed loop floor noise corresponds to the fraction of seismic noise reinjected by using the position sensors for the DC control and can, in principle, be reduced by a steeper low pass filtering of the LVDT signal at  $f > f_{\text{merge}}$  and by lowering  $f_{\text{merge}}$ : both this solution have drawbacks and need a careful implementation.

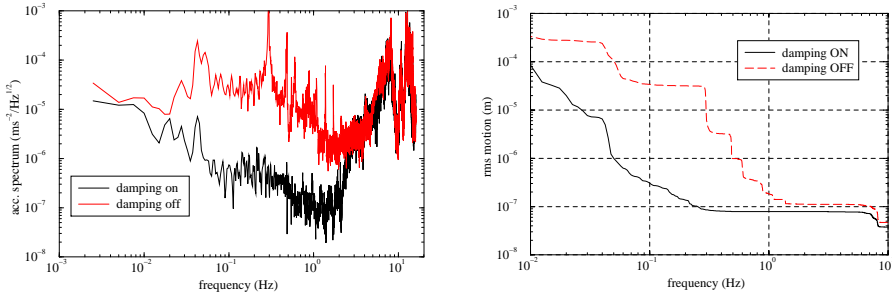


Figure 9. Performance of the inertial control ( $X, Y, \Theta$  loops closed) of the superattenuator, measured on the top of the IP: the left plot shows the acceleration spectral density as measured by the *virtual* accelerometer  $X$  (translation). The right plot shows the effect of the feedback on the RMS residual motion of the IP as a function of the frequency.

Preliminary measurements of the displacement of the mirror with respect to ground have been performed in air, using an LVDT position sensor. The residual RMS mirror motion in 10 sec. is<sup>c</sup>:

$$x_{\text{RMS}}(0.1 \text{ Hz}) \leq 3 \mu\text{m}. \quad (13)$$

When the damping is on such a measurement can provide only an upper bound because the LVDT output is dominated by the seismic motion of the ground.

## 7 Conclusions

In this lecture we have tried to outline how to face the problem of reducing the free motion of the suspended optical components of the VIRGO interferometer, associated to the resonances of the suspension. This is only the beginning: once the motion of the mirrors is reduced to a few microns, the lower control stages can operate to *lock* the interferometer in the correct operation state.

## Acknowledgments

The author wishes to thank all the people of the Pisa and Florence VIRGO Groups. Among them, special thanks to Diego Passuello, Alberto Gennai and

<sup>c</sup>This number has been obtained with a simpler feedback design, less *aggressive* than the one of fig. 8: the gain raised as  $1/f$  (pure viscous damping force), the crossover frequency was 30 mHz and no compensation of the dips was needed.

Andrea Marin.

## References

1. P.R.Saulson, *Fundamentals of interferometric gravitational wave detectors*, World Scientific (1994).
2. G.Losurdo for Pisa VIRGO Group, Proc. of the *Second E.Amaldi Conference on Gravitational Waves*, CERN, Geneva, 1-4 July 1997, eds. E.Coccia, G.Pizzella, G.Veneziano , World Scientific (1998).
3. F.Frasconi, *et al.*, Performances of the R&D superattenuator chain of the VIRGO experiment, to be published in the proceedings of the *XXXIVth Rencontres de Moriond* (1999).
4. A.Giazotto, this volume.
5. G.Losurdo, *et al.*, *Rev. Sci. Instrum.*, **70** (5), 2507-2515 (1999).
6. S.Braccini, *et al.*, *Rev. Sci. Instrum.*, **66** (3), 2672-2676 (1995).
7. S.J.Richman, J.A.Giaime, D.B.Newell, R.T.Stebbins, P.L.Bender, J.E.Faller, *Rev. Sci. Instrum.*, **69** (6), 2531 (1998).
8. A.Gennai, *et al.*, *A control model for the inverted pendulum*, VIRGO Note VIR-TRE-PIS-4900-102 (1997).
9. G.Losurdo, *Ultra-low frequency inverted pendulum pre-isolator for the VIRGO test mass suspension*, PhD Thesis, Scuola Normale Superiore, Pisa (1998).
10. G.Losurdo, in the Proceedings of the *Third E.Amaldi Conference on Gravitational Waves Experiment*, Caltech, Pasadena, 12-16 July 1999, gr-qc/9911044 (1999).
11. A.Gennai, G.Losurdo, A.Marin, D.Passuello, *Inertial damping of the superattenuator*, VIRGO Note VIR-TRE-PIS-4900-104 (1999).

## INSTRUCTIONS FOR PRODUCING A CAMERA-READY MANUSCRIPT USING WORLD SCIENTIFIC PUBLISHING STYLE FILES

C. W. LEE AND YOLANDE

*World Scientific Publishing Co., Inc, 1060 Main Street, River Edge NJ 07661,  
USA*

*E-mail: [wspc@wspc.com](mailto:wspc@wspc.com)*

ELSIE TAN, JESSIE TAN AND R. SANKARAN

*World Scientific Publishing Co Ltd, 57 Shelton Street, Covent Garden, London  
WC2H 9HE, England*

*E-mail: [wspc@wspc.ox.uk](mailto:wspc@wspc.ox.uk)*

This is where the abstract should be placed. It should consist of one paragraph and give a concise summary of the material in the article below. Replace the title, authors, and addresses within the curly brackets with your own title, authors, and addresses. You may have as many authors and addresses as you wish. It's preferable not to use footnotes in the abstract or the title; the acknowledgments for funding bodies etc. are placed in a separate section at the end of the text.

### 1 Guidelines

#### 1.1 Producing the Hard Copy

The hard copy may be printed using the advice given in the file *spread.1st*, which is repeated in this section. You should have three files in total.<sup>a</sup> *readme.txt* — the preliminary guide.

*ws-p8-50x6-00.cls* — the class file that provides the higher level latex commands for the proceedings. Don't change these parameters.

*ws-p8-50x6-00.tex* — the main text. You can delete our sample text and replace it with your own contribution to the volume, however we recommend keeping an initial version of the file for reference. Strip off any mail headers and then latex the tex file. The command for latexing is `latex ws-p8-50x6-00`, do this twice to sort out the cross-referencing.

If you wish to use some other form of word-processor, some guidelines are given in Sec. 1.2 below. These files will work with standard `latex2e`. If

---

<sup>a</sup>You can obtain these files from our WWW pages at:  
<http://www.wspc.co.uk/wspc/Styles/procs/procsread1st.html>  
[http://www.wspc.com.sg/others/style\\_files/procsread1st.html](http://www.wspc.com.sg/others/style_files/procsread1st.html) or by ftp from  
[ftp://ftp.wspc.com.sg/pub/style\\_files/proceedings/SPROCL2E/](ftp://ftp.wspc.com.sg/pub/style_files/proceedings/SPROCL2E/).

there is an abbreviation defined in the new definitions at the top of the file *ws-p8-50x6-00.tex* that conflicts with one of your own macros, then delete the appropriate command and revert to longhand. Failing that, please consult your local *texpert* to check for other conflicting macros that may be unique to your computer system. Page numbers are included at the bottom of the page for your guidance. Do not worry about the final pagination of the volume which will be done after you submit the paper.

### 1.2 Using Other Word-Processing Packages

If you want to use some other form of word-processor to construct your output, and are using the final hard copy version of these files as guidelines; then please follow the style given here for headings, table and figure captions, and the footnote and citation marks. For this size of volume, the final page dimensions will be 8.5 by 6 inches (21.5 by 15.25 cm) however you should submit the copy on standard A4 paper. The text area, which includes the page numbers should be 7 by 4.7 inches (17.75 by 12 cm). The text should be in 10pt roman for the title, section heads and the body of the text, and 9pt for the authors' names and addresses. Please use capitals for the title and authors, bold face for the title and headings, and italics for the subheadings. The abstract, footnotes, figure and table captions should be in 8pt.

It's also important to reproduce the spacing of the text and headings as shown here. Text should be slightly more than single-spaced; use a baselineskip (which is the average distance from the base of one line of text to the base of an adjacent line) of 13 pts and 10 pts for footnotes. All headings should be separated from the text preceding it by a baselineskip of about 26 pts and use a baselineskip of about 18 pts for the following text.

Paragraphs should have a first line indented by about 0.25in (6mm) except where the paragraph is preceded by a heading and the abstract should be indented on both sides by 0.25in (6mm) from the main body of the text.

### 1.3 Headings and Text and Equations

Please preserve the style of the headings, text fonts and line spacing to provide a uniform style for the proceedings volume.

Equations should be centered and numbered consecutively, as in Eq. (1), and the *eqnarray* environment may be used to split equations into several lines, for example in Eq. (3), or to align several equations. An alternative method is given in Eq. (2) for long sets of equations where only one referencing equation number is wanted.

Table 1. Experimental Data bearing on  $\Gamma(K \rightarrow \pi\pi\gamma)$  for the  $K_S^0$ ,  $K_L^0$  and  $K^-$  mesons.

	$\Gamma(\pi^-\pi^0) s^{-1}$	$\Gamma(\pi^-\pi^0\gamma) s^{-1}$		
Process for Decay				
$K^-$	$1.711 \times 10^7$	$2.22 \times 10^4$ (DE $1.46 \times 10^3$ )	No (IB)-E1 interference seen but data shows excess events relative to IB over $E_\gamma^* = 80$ to 100 MeV	

In latex, it is simplest to give the equation a label, as in Eq. (1) where we have used `\label{eq:murnf}` to identify the equation. You can then use the reference `\ref{eq:murnf}` when citing the equation in the text which will avoid the need to manually renumber equations due to later changes. (Look at the source file for some examples of this.)

The same method can be used for referring to sections and subsections.

#### 1.4 Tables

The tables are designed to have a uniform style throughout the proceedings volume. It doesn't matter how you choose to place the inner lines of the table, but we would prefer the border lines to be of the style shown in Table 1. The top and bottom horizontal lines should be single (using `\hline`), and there should be single vertical lines on the perimeter, (using `\begin{tabular}{|...|}`). For the inner lines of the table, it looks better if they are kept to a minimum. We've chosen a more complicated example purely as an illustration of what is possible.

The caption heading for a table should be placed at the top of the table.

#### 1.5 Figures

If you wish to 'embed' a postscript figure in the file, then remove the % mark from the declaration of the postscript figure `epsfbox` within the figure description and change the filename to an appropriate one. Also remove the comment % mark from the `epsfxsize` command and specify the required width of the figure. System will automatically enlarge or reduce the figure based on the `x-size` provided with `epsfxsize` command. You may need to play around with this as different computer systems appear to use different commands. If you like to have an empty box size to the image you can just fill in the `x`, `y`

*size* against the command *figurebox*, which has three arguments. The third argument is for actual figure name.

Next adjust the scaling of the figure until it's correctly positioned, and remove the declarations of the lines and any anomalous spacing.

If you prefer to use some other method then it's very important to leave the correct amount of vertical space in the figure declaration to accomodate your figure (remove the lines and change the *vspace* in the example.) Send the hard copy figures on separate pages with clear instructions to match them to the correct space in the final hard copy text. Please ensure the final hard copy figure is correctly scaled to fit the space available (this ensures the figure is legible.)

The caption heading for a figure should be placed below the figure.

### 1.6 Limitations on the Placement of Tables, Equations and Figures

Very large figures and tables should be placed on a page by themselves. One can use the instruction `\begin{figure}[p]` or `\begin{table}[p]` to position these, and they will appear on a separate page devoted to figures and tables. We would recommend making any necessary adjustments to the layout of the figures and tables only in the final draft. It is also simplest to sort out line and page breaks in the last stages.

### 1.7 Acknowledgments, Appendices, Footnotes and the Bibliography

If you wish to have acknowledgments to funding bodies etc., these may be placed in a separate section at the end of the text, before the Appendices. This should not be numbered so use `\section*{Acknowledgments}`.

It's preferable to have no appendices in a brief article, but if more than one is necessary then simply copy the `\section*{Appendix}` heading and type in Appendix A, Appendix B etc. between the brackets.

Footnotes are denoted by a letter superscript in the text,<sup>b</sup> and references are denoted by a number superscript. We have used `\bibitem` to produce the bibliography. Citations in the text use the labels defined in the `\bibitem` declaration, for example, the first paper by Jarlskog <sup>1</sup> is cited using the command `\cite{ja}`.

If you more commonly use the method of square brackets in the line of text for citation than the superscript method, please note that you need to adjust the punctuation so that the citation command appears after the punctuation mark.

---

<sup>b</sup>Just like this one.

### 1.8 Final Manuscript

The final hard copy that you send must be absolutely clean and unfolded. It will be printed directly without any further editing. Use a printer that has a good resolution (300 dots per inch or higher). There should not be any corrections made on the printed pages, nor should adhesive tape cover any lettering. Photocopies are not acceptable.

The manuscript will not be reduced or enlarged when filmed so please ensure that indices and other small pieces of text are legible.

## 2 Sample Text

The following may be (and has been) described as ‘dangerously irrelevant’ physics. The Lorentz-invariant phase space integral for a general n-body decay from a particle with momentum  $P$  and mass  $M$  is given by:

$$I((P - k_i)^2, m_i^2, M) = \frac{1}{(2\pi)^5} \int \frac{d^3 k_i}{2\omega_i} \delta^4(P - k_i). \quad (1)$$

The only experiment on  $K^\pm \rightarrow \pi^\pm \pi^0 \gamma$  since 1976 is that of Bolotov *et al.*<sup>3</sup> There are two necessary conditions required for any acceptable parametrization of the quark mixing matrix. The first is that the matrix must be unitary, and the second is that it should contain a CP violating phase  $\delta$ . In Sec. 1.2 the connection between invariants (of form similar to  $J$ ) and unitarity relations will be examined further for the more general  $n \times n$  case. The reason is that such a matrix is not a faithful representation of the group, i.e. it does not cover all of the parameter space available.

$$\begin{aligned} \mathbf{K} = & \text{Im}[V_{j,\alpha} V_{j,\alpha+1}^* V_{j+1,\alpha}^* V_{j+1,\alpha+1}] \\ & + \text{Im}[V_{k,\alpha+2} V_{k,\alpha+3}^* V_{k+1,\alpha+2}^* V_{k+1,\alpha+3}] \\ & + \text{Im}[V_{j+2,\beta} V_{j+2,\beta+1}^* V_{j+3,\beta}^* V_{j+3,\beta+1}] \\ & + \text{Im}[V_{k+2,\beta+2} V_{k+2,\beta+3}^* V_{k+3,\beta+2}^* V_{k+3,\beta+3}] \\ \mathbf{M} = & \text{Im}[V_{j,\alpha}^* V_{j,\alpha+1} V_{j+1,\alpha} V_{j+1,\alpha+1}^*] \\ & + \text{Im}[V_{k,\alpha+2} V_{k,\alpha+3}^* V_{k+1,\alpha+2}^* V_{k+1,\alpha+3}] \\ & + \text{Im}[V_{j+2,\beta}^* V_{j+2,\beta+1} V_{j+3,\beta} V_{j+3,\beta+1}^*] \\ & + \text{Im}[V_{k+2,\beta+2} V_{k+2,\beta+3}^* V_{k+3,\beta+2}^* V_{k+3,\beta+3}], \end{aligned} \quad (2)$$



Figure 1. A generalized cactus tree: the confluent transfer-matrix  $S$  transforms the state function  $f(x)$  and  $f(z)$  into  $f(x)$ .

where  $k = j$  or  $j + 1$  and  $\beta = \alpha$  or  $\alpha + 1$ , but if  $k = j + 1$ , then  $\beta \neq \alpha + 1$  and similarly, if  $\beta = \alpha + 1$  then  $k \neq j + 1$ .<sup>c</sup> There are only 162 quark mixing matrices using these parameters which are to first order in the phase variable  $e^{i\delta}$  as is the case for the Jarlskog parametrizations, and for which  $J$  is not identically zero. It should be noted that these are physically identical and form just one true parametrization.

$$\begin{aligned}
 T = & \text{Im}[V_{11}V_{12}^*V_{21}^*V_{22}] \\
 & + \text{Im}[V_{12}V_{13}^*V_{22}^*V_{23}] \\
 & - \text{Im}[V_{33}V_{31}^*V_{13}^*V_{11}].
 \end{aligned} \tag{3}$$

---

<sup>c</sup>An example of a matrix which has elements containing the phase variable  $e^{i\delta}$  to second order, i.e. elements with a phase variable  $e^{2i\delta}$  is given at the end of this section.

## Acknowledgments

This is where one places acknowledgments for funding bodies etc. Note that there are no section numbers for the Acknowledgments, Appendix or References. Furthermore, the system will automatically generate the heading for the reference section.

## Appendix

We can insert an appendix here and place equations so that they are given numbers such as Eq. (4).

$$x = y. \quad (4)$$

## References

1. C Jarlskog in *CP Violation*, ed. C Jarlskog (World Scientific, Singapore, 1988).
2. L. Maiani, *Phys. Lett. B* **62**, 183 (1976).
3. J.D. Bjorken and I. Dunietz, *Phys. Rev. D* **36**, 2109 (1987).
4. C.D. Buchanan *et al*, *Phys. Rev. D* **45**, 4088 (1992).